

Victoria Prieto<sup>1,2</sup>, Maxime Forte<sup>1</sup> & Erwin R. Gowree<sup>2</sup>

<sup>1</sup>ONERA Toulouse <sup>2</sup>ISAE-SUPAERO

#### **Abstract**

The present study examines the effect of surface roughness on boundary-layer transition over a swept wing. First, the mechanisms driving the transition on the reference smooth configuration for low angles of attack were investigated. Subsequently, similar experiments were conducted for three different distributed roughness heights. The results of the experiments demonstrate a clear advance in the transition position as the roughness height increases. This can be attributed to the additional amplification of the existing instabilities, which are predominantly Tollmien-Schlichting waves. Finally, the linear stability theory and the  $e^N$  method coupled with these results are used to propose a semi-empirical model that allows predicting the influence of surface roughness on the growth rate of instability mode leading to boundary layer transition.

**Keywords:** boundary layer, laminar-turbulent transition, surface roughness, Tollmien-Schlicthing, Linear Stability Theory

## 1. Context and objectives

Nowadays, research is extensively focused on minimising fuel consumption through drag reduction mechanisms, which represents a major issue towards the limitation of the carbon footprint in civil aviation. 50% of the total drag is due to skin friction, highly influenced by turbulent boundary layers, which leads to multiple solutions seeking to reduce its effect. Among these solutions, there are the laminar wings, that are aimed at extending the laminar zone over the wing, allowing the reduction of the skin friction drag. To further advance in the development of these solutions, it is necessary to properly understand the laminar-turbulent transition and the factors influencing this phenomenon.

The boundary layer can be subjected to external perturbations of different nature: turbulence, acoustics and, in particular, surface roughness and vibration [1]. The initial amplitude of the perturbations introduced into the boundary layer during the receptivity phase determines the transition mechanism [2]. For a two-dimensional boundary layer subjected to a low turbulence intensity, the instabilities leading to transition are Tollmien-Schlichting waves, while for three-dimensional boundary layers, for instance on a swept wing, three-dimensional instabilities, known as crossflow instabilities may also appear. In contrast to localised discrete roughness, which has been historically studied both experimentally [3, 4] and numerically [5, 6], the influence of distributed surface roughness on the transition is less understood.

Some of the existing work focuses on the effect of low-density rough surfaces such as the experiments conducted by Von Doenhoff and Braslow [7], where evenly distributed isolated elements were used. In contrast, other studies have investigated the effect of higher density roughness, such as Jeong et al. [8]. Some attempts have been made to model the transition in the presence of roughness. For instance, Crouch [9] focused on crossflow-driven transition, while Ducaffy [10] proposed a semi-empirical model based on experiments conducted over a flat plate. Nevertheless, there is

currently no existing model that can predict the onset of transition for more complex aerodynamic surfaces, in the presence of pressure gradient and three-dimensional effects on the boundary layer.

In this context, the aim of the present study is to further investigate the influence of the surface roughness on a swept wing, where both Tollmien-Schlichting waves and crossflow instabilities may be present, although in this paper only the former is studied. To achieve this, the amplification of the instabilities present within the boundary-layer during transition is experimentally studied for different randomly distributed surface roughness, angles of attack and Reynolds numbers. The results of these experiments, when combined with a numerical linear stability analysis, will provide valuable insight into the transition mechanisms involved and lead to the development of a semi-empirical model that can be used to predict transitions in similar configurations. This study is an extension of the work started at ONERA in 2018 by Ducaffy [11], during which a first experimental setup on a flat plate allowed to highlight the effect of some roughness parameters on the advancement of the transition induced by Tollmien-Schlichting waves.

# 2. Methodology

## 2.1 Wind tunnel facility and wing model

This study was conducted in the F2 wind tunnel at ONERA Fauga-Mauzac, which is a subsonic closed-return wind tunnel with a maximum speed of 100 m/s and a test section of 5 m x 1.8 m x 1.4 m (length x height x width). The wind tunnel in question offers a remarkably low level of turbulence, with an intensity of less than 0.04% at its maximum velocity across a frequency range of [60 Hz, 5 kHz].

The airfoil model under consideration, designated DTP-B, is a semi-infinite swept wing or 2.5D wing, aimed at minimising the spanwise pressure gradient. The wing has three possible sweep angles,  $\varphi$ , of 40°, 50°, and 60°, although its span, s, remains constant and equal to 1.605 m in the vertical direction (see figure ,1a), thanks to the extension of wingtips. The model's geometry, initially designed by Reneaux [12], comprises an assymmetric profile with a constant chord length, c=700mm, perpendicularly to the leading edge, and with a maximum thickness of 94.1 mm. The geometry of the airfoil, presented in figure 1b, is available for further study upon request.

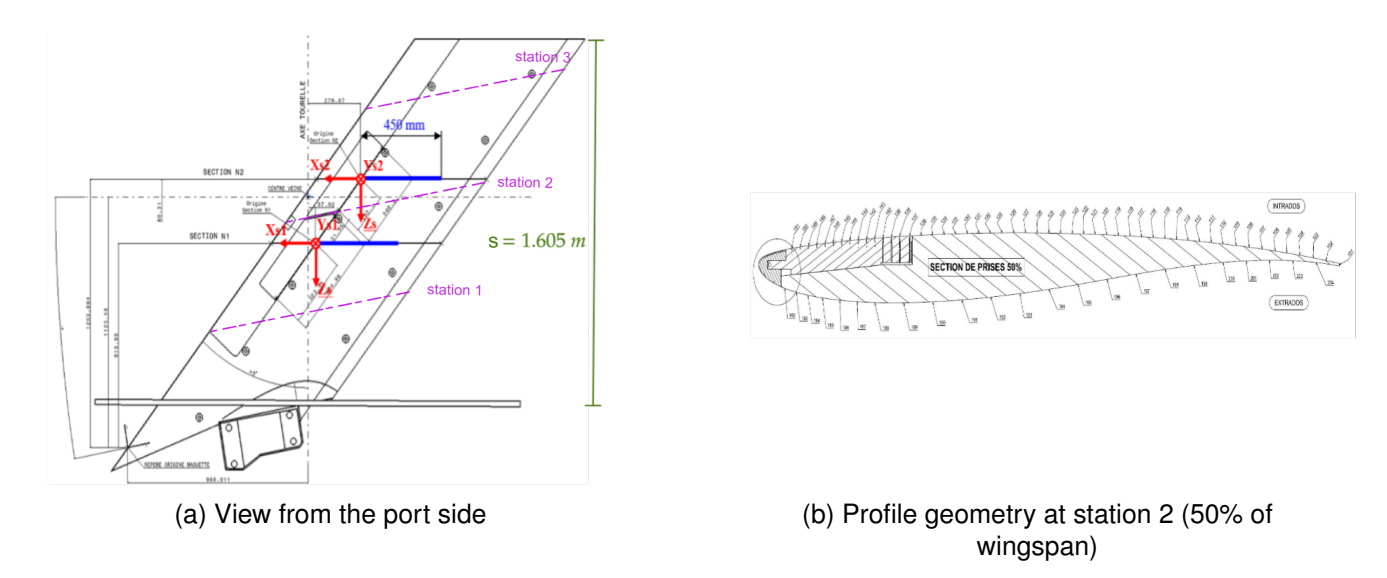


Figure 1 – DTP-B geometry and profile

The model was initially conceived and manufactured by ONERA in 1995 [13] using aluminium alloy. It comprises of two parts: the main body and a detachable leading edge. The latter has been modified for the purposes of this experimental campaign, with the incision for two inserts downstream of

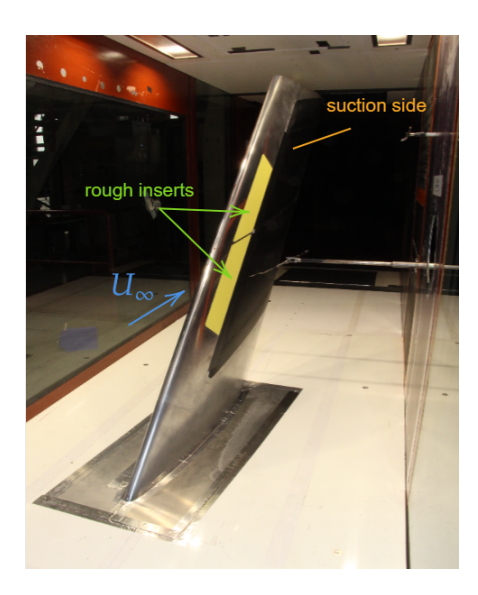


Figure 2 – Overview of DTP-B mounted in the test section

the leading edge of the model as shown in yellow in figure 2. The two incisions, located between 10% and 26.5% of the chord, allowed the placement of two detachable inserts which were covered by sandpaper. Three distinct levels of roughness were studied. The sole differentiating factor being the grain size, which consequently influenced the surface-average roughness,  $S_a$ . The values for this parameter were 14  $\mu m$ , 19  $\mu m$  and 27  $\mu m$  for P240, P180 and P120 respectively. Note that the rough inserts were placed so that the average roughness plane (see figure 4) was aligned with the original smooth reference surface, thus reducing the possibility of localised defects such as a gap or a forward step.

The wing was also equipped with 178 pressure taps distributed over three stations aligned with the flow direction when the sweep angle is 50°, with the taps located at 25%, 50% and 75% wingspan (see figure 1). Stations 1 and 3, for a 25% and 75% of the wingspan, respectively, are equipped with 37 pressure taps on the suction side. In contrast, station 2, 50% of the span, is equipped with 104 pressure taps distributed between the suction and pressure sides, as shown in figure 1b.

Figure 3 shows the pressure coefficients measured over the three stations. This figure shows that for the stations at 25% and 50% of the chord, there is minimal spanwise velocity gradient and the 2.5D approximation holds, but the station further outward experiences 3D effects. From all the stations provided, in this paper only the pressure measurements captured at station 2 will be considered for further boundary-layer calculation and stability analysis. Figure 3b depicts the pressure coefficients for a fixed Reynolds number of  $3.3 \cdot 10^6 \ m^{-1} \ (U_{\infty} \approx 50 \ m/s)$  at various angles of attack. Unlike on conventional wings, here the suction peak is higher for lower values of angle of attack. This allows us to study the effect of pressure gradient on the amplification of instability modes in the presence of roughness, unlike previous studies which conducted in the absence of pressure gradient.

In the present study, freestream velocities were varied between 30 and 80 m/s, which corresponds to Reynolds numbers between  $2.1 \cdot 10^6~m^{-1}$  and  $5.5 \cdot 10^6~m^{-1}$ , while the sweep angle was fixed at 40°. The model was mounted vertically in the test section as shown in figure 2, situated at a distance of 1730 mm downstream of the entry of the test section. Different angles of attack,  $\alpha$ , were studied, ranging between -1° to 6°, with the value selected depending on the transition scenario. It must be noted, that in this work all measurements were performed over the suction side.

## 2.2 Flow measurement techniques

Three type of measurements were made: pressure, infrared thermography and hot-wire anemometry measurements. Three PSI differential pressure scanners with a range of  $\pm$  34500 Pa were used to

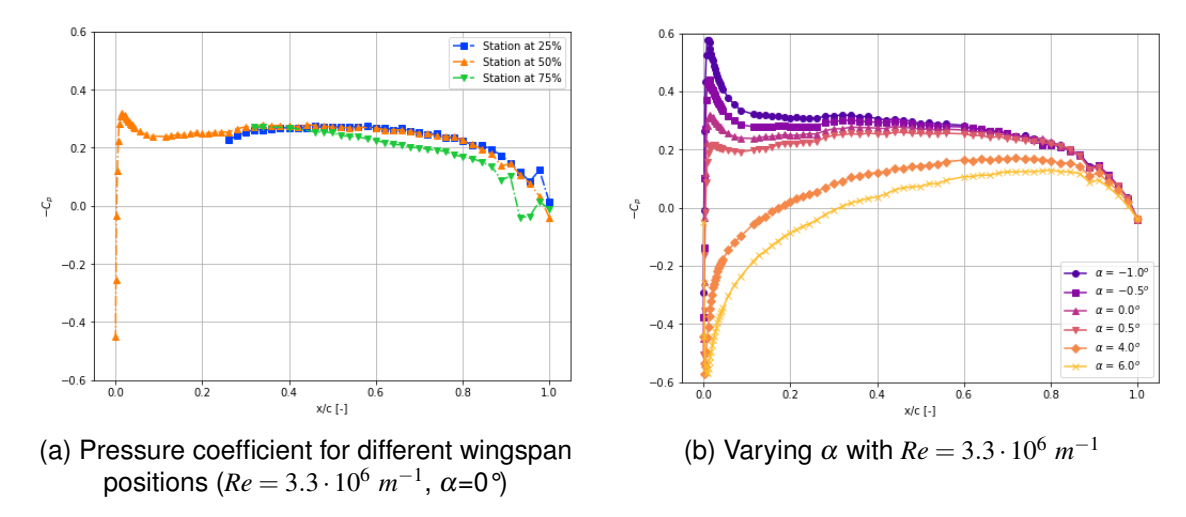


Figure 3 – Pressure coefficient over the model

measure the static pressure presented previously. For the infrared thermography, an IRC900 camera was placed on the port-side of the test section. The results depicted from the latter are however not presented in this paper. Lastly, velocity measurements were conducted using constant-temperature hot-wire anemometry. Specifically, a Dantec Streamline with a CTA 90C10 module and 55P15 boundary layer probes were utilised. Hot-wire measurements in the boundary layer were first conducted for a fixed wall normal position traversed along the chordwise direction. Then, measurements traversed along the normal to the streamwise direction were also performed for selected chordwise positions. The sampling frequency was set to 25 kHz with  $2.5 \cdot 10^4$  samples for each measurement point, which was increased to  $10^6$  for specific cases requiring spectral analysis. The hot wire probe was calibrated in-situ with a pitot-tube mounted upstream of the test-section so as to avoid blockage interference from the model and the test section walls.

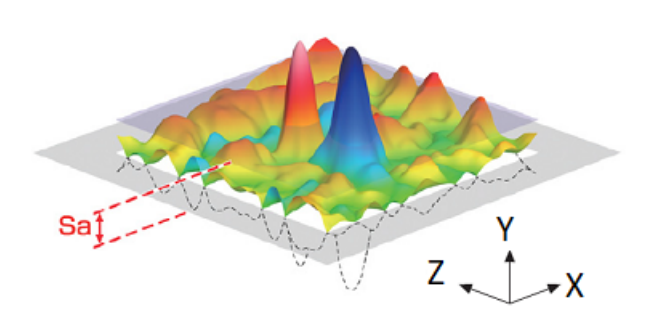
# 2.3 Surface roughness characterisation

The determination of surface roughness is a challenging task. In order to achieve this, a number of parameters were chosen, each offering a different type of information which can be used to compare surfaces with different roughness topography. The definition of these parameters can be either two or three-dimensional, depending on the measurement technique employed.

Traditional roughness measurement techniques relied on surface contact, such as surface profilometers, which, although providing measurements down to mirons, it has major limitations inherent in tactile measurement techniques [14]. One of the major limitations is that the measurements are taken along a single plane perpendicular to roughness, which is not necessarily representative of the surface as a whole. The emergence of optical techniques such as variable focus and white light interferometry allows three-dimensional surface roughness characterisation with decent reliability. In contrast to the planar two-dimensional measurements techniques, the three-dimensional techniques uses the mean plane as a reference, as illustrated in figure 4. Due to the statistical nature of roughness characterisation, 3D analysis will provide more accurate data, although this will be at the cost of increased computational complexity.

For the sake of simplicity, in this paper we will refer to different roughness types by their average roughness height,  $S_a$ , as defined in 1. However, there are other important parameters also being considered in this study, such as the root mean square roughness,  $S_q$ , or the skewness,  $S_{sk}$ . All of these parameters were experimentally measured using the InfiniteFocus SL from Bruker Alicona, an optical surface roughness measurement instrument that employs focus variation. This approach enables the characterisation of roughness topography at high resolution, as illustrated in figure 5.

$$S_a = \frac{1}{A} \int \int_A |y(x,z)| dx dz \tag{1}$$



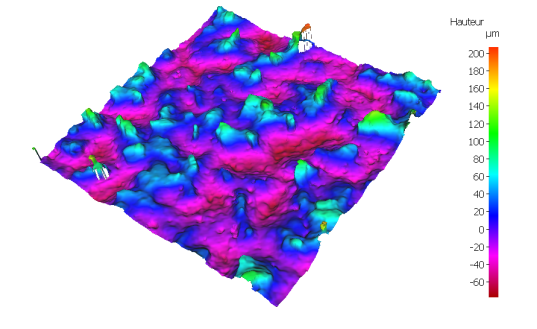


Figure  $4 - S_a$  and mean plane definition

Figure 5 – Roughness scan ( $2x2 mm^2$ )  $S_a = 27 \mu m$ 

# 2.4 Boundary layer instability growth and transition

Although several angles of attack have been studied, here only three configurations are presented, namely,  $\alpha = -0.5^{\circ}$ ,  $0^{\circ}$ , and  $0.5^{\circ}$ . These angles corresponded to cases where Tollmien-Schlichting waves were observed to be the primary instabilities. As the angle of attack increases, the crossflow instabilities became more significant, but this is outside the scope of the current study.

Furthermore, using the pressure gradients presented in figure 3b, the development of the boundary layer was computed using ONERA's in-house code, 3C3D, while applying a semi-infinite swept wing assumption. In this paper, the envelope method proposed by Arnal in 1988 [19] is employed to calculate the total amplification rate of a spatially growing wave at a given frequency, also known as the  $N_f$  factor.

$$N_f(x) = \ln\left(\frac{A(x)}{A_0}\right) = \int_{x_0}^x -\alpha_i(\eta)d\eta \tag{2}$$

where A(x) is the wave amplitude at each abscissa,  $A_0$  is the initial wave amplitude at  $x_0$  when it becomes unstable, and  $-\alpha_i$  is the spatial amplification rate. Later, by taking the maximum value of all the modes, we can obtain the envelope of amplification, known as the N-factor. This is the basis for the so-called  $e^N$  method, that will be used in this paper. This method was originally developed for low-speed flows by Smith and Gamberoni [15] and by van Ingen [16] in 1956. It was later extended to compressible flows by Mack in 1984 [17] and to three-dimensional flows by Arnal in 1994 [18]. It should be noted that the envelope method employed here represents an approximation to the solution of the Linear Stability Theory (LST). In future analysis, exact stability calculations will be performed.

Thanks to the  $e^N$  method, and using empirical criteria such as Mack's law [17], the transition position could be predicted for the reference case. In this paper, however, the transition positions for the various cases studied were measured using hot-wire anemometry and later extrapolated to the reference N-curve. This provides two  $N_T$  thresholds, which correspond to the N values depicted from the N-factor at the given transition positions. These values allow calculating the shift that the N-curve should encounter to account for the effect of roughness without changing the  $N_T$  threshold, as shown in figure 6. The calculation of such a shift is as follows,

$$\Delta N = N_T |_{smooth} - N_T |_{rough} \tag{3}$$

where  $N_T|_{smooth}$  corresponds to the threshold obtained for the smooth reference case, and  $N_T|_{rough}$  for the rough configuration. This phenomenon is known as over-amplification and results from an increase in the amplification of instabilities induced by the presence of roughness.

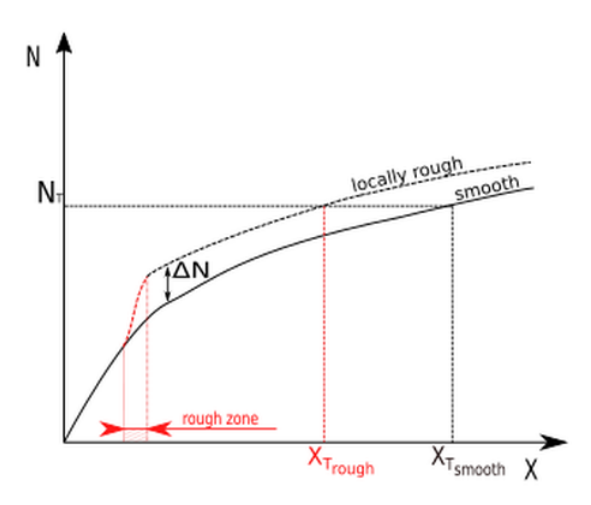


Figure 6 – Over-amplification effect ont eh  $e^N$  method

Two different types of velocity measurements were performed using hot-wire anemometry. On one hand, mean velocity profiles within the boundary layer were determined at a given chordwise position, as shown in figure 7. Due to the limitations in the near-wall alignment of the hot-wire, only partial velocity profiles could be captured. On the other hand, the velocity fluctuations were captured at a fixed wall normal position but over a refined number of chordwise position by performing a streamwise traversing, the allowed spectral analysis and the evolution of the streamwise velocity fluctuations, u', helped in tracking the rate of growth of the instability and identifying the position of secondary growth from saturation and eventual transition.

These last measurements in the streamwise direction were performed at two spanwise position corresponding to 727 mm and 968 mm from the bottom of the model, but here only the results obtained at the lowest spanwise station (N1 in figure 1a) are presented, as it was located with the region where the flow exhibited the 2.5D characteristcs. To ensure the probe was positioned at a fixed wall-normal position and to prevent the hot wire from damaging by short-circuit upon contact with the wall, a drop of resin was placed at the hot-wire prongs. This prevented contact with the model wall by maintaining a probing height within the boundary layer between 0.5 and 1 mm during the streamwise traversing, which remained constant for each measurement. Thanks to the results depicted, the transition position for both, the smooth and rough cases, could be calculated and compared with  $e^N$  method. Further details are presented in the next section.

## 3. The baseline smooth case

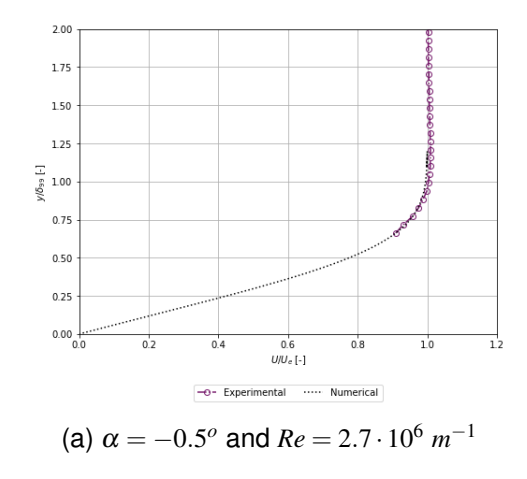
In order to assess the impact of surface roughness on the boundary layer transition, it is essential to conduct a comprehensive analysis of the baseline smooth case, providing reference measurements that will be used to asses the effect of the roughness.

#### 3.1 Mean velocity profiles

The boundary layer mean velocity profiles have been experimentally captured and compared with the numerical ones obtained from 3C3D. It is important to note that the distance between the hot wire probe and the wall during the boundary layer measurements were not measured accurately. Consequently, the numerical results were used to re-adjust the position of the probe with respect to the wall. This was accomplished by assuming that the initial point of the measurement,  $y_0|_{exp}$ , corresponds to the y-value of the numerical boundary layer,  $y|_{num}$ , where  $U(y|_{num}) = U(y_0|_{exp})$ .

Due to the constraints of the experimental setup, the mean velocity profiles were not measured normal to the model's wall but rather perpendicular to the flow. For this reason, the point at which the

measurements were taken was x/c = 0.396, where the curvature of the model is reduced compared to other chordwise positions. Figure 7 depicts the comparison of the boundary layer profiles for two distinct Reynolds numbers and angles of attack. Both sets of results demonstrate a high degree of agreement between the experimental data and the numerical calculations, with the agreement being more pronounced for the lower Reynolds numbers. More importantly, they show that all measurements made, including those in the streamwise scans at fixed wall normal position, were conducted within the boundary layer as desired.



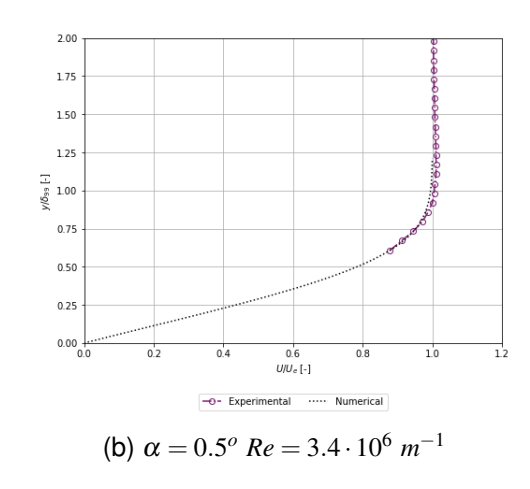
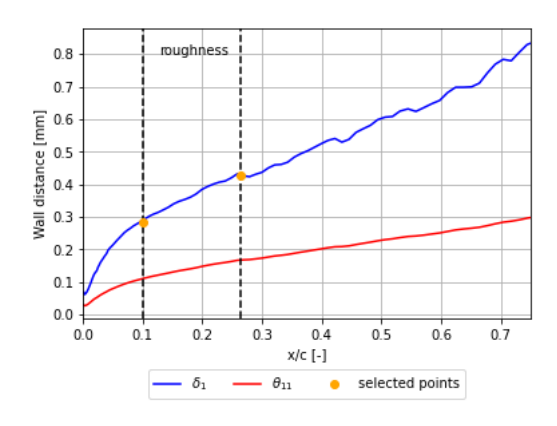


Figure 7 – Boundary layer experimental-numerical comparison for the smooth reference case at x/c = 0.396

Furthermore, the numerical analysis on the boundary layer enables the calculation of integral parameters, including the streamwise displacement thickness,  $\delta_1$ , and the momentum thickness,  $\theta_{11}$ . Figure 8 illustrates the evolution of these parameters in the streamwise direction for the reference case. From this evolution, a mean displacement thickness, denoted by  $\bar{\delta}_1$ , is calculated by taking the mean value between the displacement thickness upstream and downstream the roughness insert, at 10 and 26.5% of the chord respectively. This procedure was repeated for all the cases, and the evolution with the Reynolds number and angle of attack are shown in figure 9. The error bars in figure 9 represent the  $\delta_1$  values calculated at the upstream and downstream of the roughness insert, and it can be observed that there is a minimal dependency between the angle of attack and the value of  $\bar{\delta}_1$ . As the Reynolds number increases, the value of  $\bar{\delta}_1$  decreases as expected.



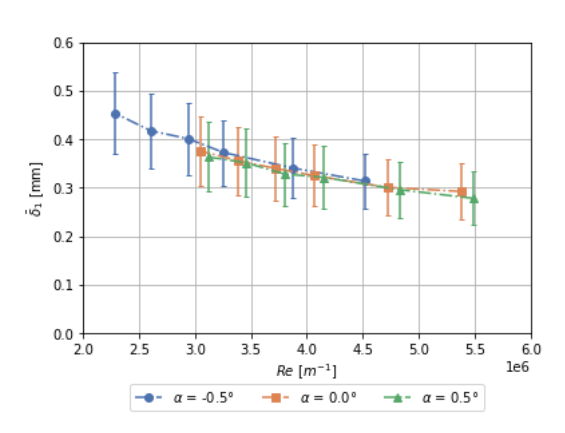


Figure 8 –  $\delta_1$  and  $\theta_{11}$  variation on the streamwise direction  $(Re = 3.4 \cdot 10^6 \ m^{-1} \ {\rm and} \ \alpha = 0^o)$ 

Figure 9 – Average displacement thickness values,  $\bar{\delta}_1$ , for the different cases studied

## 3.2 Boundary-layer transition on the baseline smooth case

Although for small angles of attack the transition is mainly dominated by Tollmien-Schlichting waves, crossflow modes are still active. This is illustrated in figure 10, where the N-factor incorporates contributions from both Tollmien-Schlichting waves and crossflow instabilities, particularly in the vicinity of the leading edge. However, as mentioned earlier, the scope of this paper is limited to the study of the boundary-layer transition driven by Tollmien-Schichting waves. Consequently, only the N-factor resulting from these instabilities is considered for the determination of the  $N_T$  threshold values, which is calculated using the transition positions measured experimentally, as illustrated in figure 10.

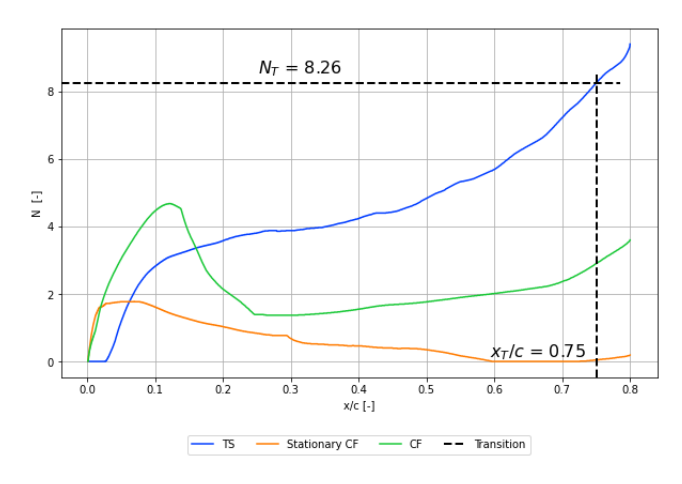


Figure 10 – Contributions of the different instabilities to the N-factor ( $Re = 3.4 \cdot 10^6 \ m^{-1}$ ,  $\alpha = 0^{\circ}$ )

Figure 11 shows the non-dimensional streamwise velocity fluctuations,  $u'/U_{\infty}$ , at different positions within the boundary layer for the reference smooth case at  $\alpha=0^{\circ}$ . These fluctuations are measured in the form of the root mean square (rms) of the velocity and allow the determination of the transition position using Methel's criterion [20]. This criterion states that the transition occurs when the nondimensional velocity fluctuations,  $u'/U_0$ , first begin to increase with a slope equal to or greater than  $2 \cdot 10^{-4}$  mm and continue to reach this threshold for two consecutive measurement stations.

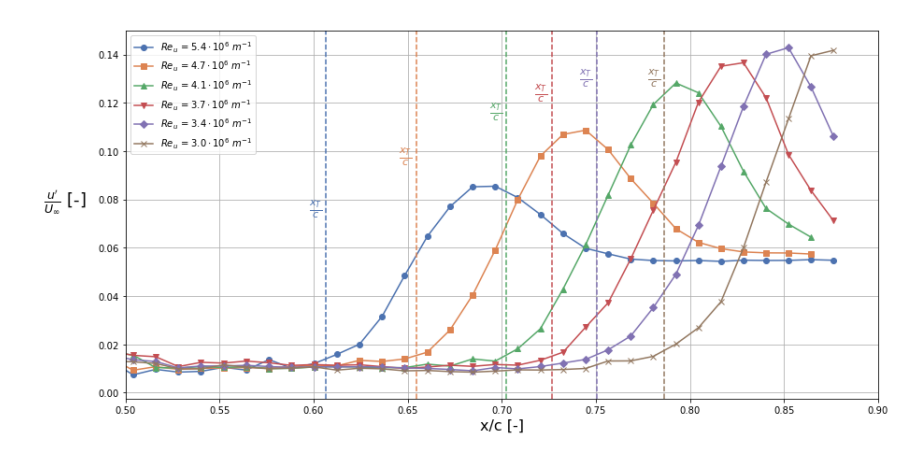


Figure 11 – Example of streamwise velocity fluctuations evolution at y = 0.5 mm to determine the transition position on the smooth reference model (Re =  $3.4 \cdot 10^6 \ m^{-1}$ ,  $\alpha$ =0°)

Figure 12a depicts the transition positions and associated Reynolds numbers for the various cases under consideration. As anticipated, the transition position is found to be shifted upstream with increasing Reynolds numbers. Furthermore, the greater the angle of attack, the later the transition occurs, rendering the case where  $\alpha=0.5^{\circ}$  the most promising for studying the effects of roughness for higher Reynolds numbers, whereas for lower Reynolds numbers  $\alpha=-0.5^{\circ}$  provided a larger extent of laminar flow. The N-factors calculated for each specific case using the LST, in conjunction with

the transition positions presented, allow for the calculation of the critical  $N_T$  values of reference (for Tollmien-Schlichting waves) showed in figure 12b. It is important to note that for  $\alpha=0^{o}$ , the  $N_T$  values for the two highest Reynolds numbers could not be calculated due to some unexpected issues in the numerical stability calculations. These two cases will be revisited in the future once the exact stability calculations are conducted.

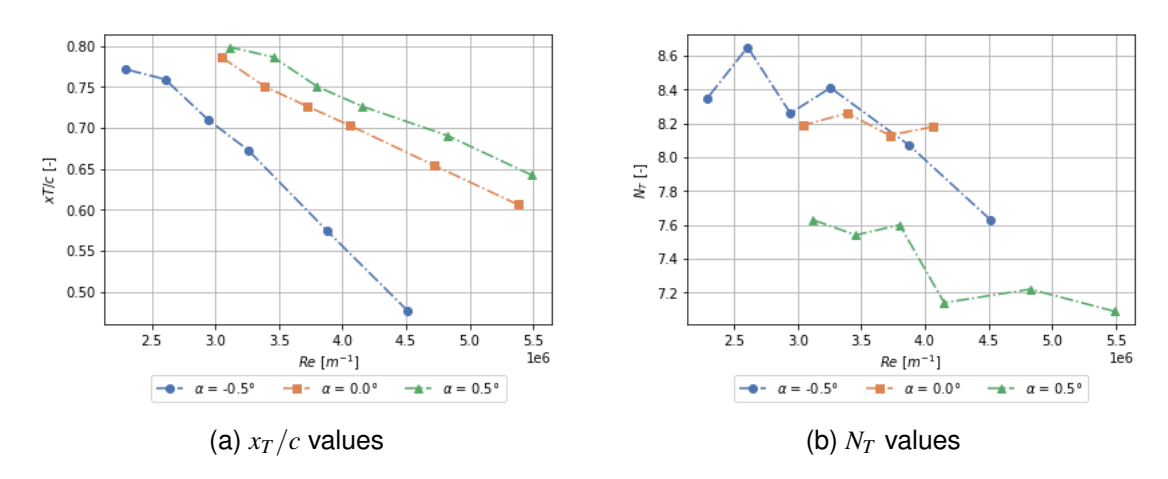


Figure 12 – Transition positions depicted from the smooth reference case at three angles of attack for various Reynolds numbers

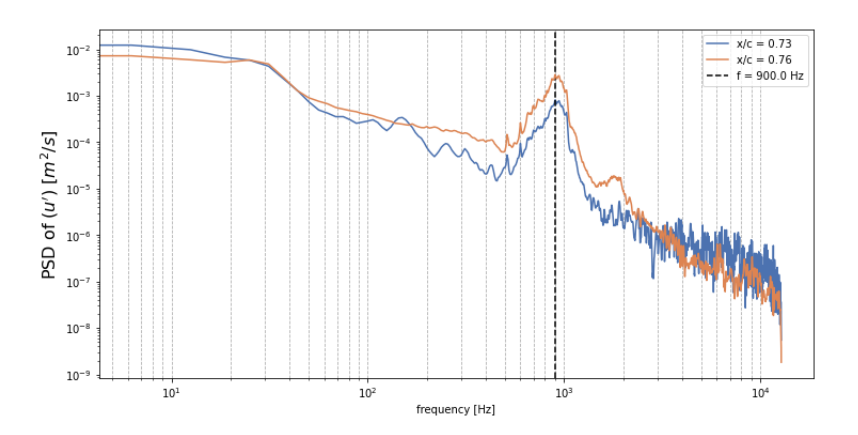


Figure 13 – PSD of u' at Re=  $3.4 \cdot 10^6 \ m^{-1}$  and  $\alpha = 0^o$  for x/c = 0.73-0.76

Moreover, the power spectral densities (PSD) of u' for a selected smooth case of  $Re = 3.4 \cdot 10^6~m^{-1}$  and  $\alpha = 0^o$  are presented in figure 13. The calculations were conducted for two position situated in the proximity of the transition position. The first, x/c = 0.73, is obtained within the linear growth region, showing a bump centered around 900 Hz. The second, x/c = 0.76, at the beginning of the non-linear region, as can be deduced from the second bump appearing around 1800 Hz, which is a harmonic of the primary mode and characteristic of secondary instabilities. The two PSD thus yield the typical wave-packet behaviour expected from Tollmien-Schlichting waves. This is therefore consistent with the observations made from the numerical analysis, where the most amplified frequency found at x/c = 0.75 (beginning of transition) is around 1050 Hz.

Finally, table 1 provides a summary of instability and transition characteristics of the reference smooth case at  $\alpha=0^{o}$ . For each Reynolds number, several parameters are displayed: the transition position,  $x_{T}$ , the Reynolds number based on the transition location,  $Re_{x_{T}}$ , the critical N-factor,  $N_{T}$ , the frequency of the most amplified mode at the transition position both, measured experimentally,  $F_{exp}$ , and according to the N-factor envelope method,  $F_{PARAB}$ . The envelope method tends to overestimate the most amplified frequencies, yet remains sufficiently close to the experimentally value, despite the inherent limitations of the method. The values presented in this table serve as a reference for comparison with

the results of the experiments using rough inserts. For the sake of clarity, only the results at  $\alpha = 0^{\circ}$ are presented in table 1.

$Re(x10^{-6}) [m^{-1}]$	$x_T [mm]$	$x_T/c$	$Re_{x_T} (x10^{-6})$	$N_T$	$F_{exp}$ [Hz]	$F_{PARAB}$ $[Hz]$
5.4	554.09	0.61	2.98	/	1840	/
4.7	598.04	0.65	2.82	/	1640	/
4.1	641.96	0.70	2.61	8.18	1140	1400
3.7	663.90	0.73	2.47	8.13	975	1250
3.4	685.84	0.75	2.32	8.26	900	1050
3.1	718.71	0.79	2.19	8.19	/	850

Table 1 – Summary of the reference smooth case for  $\alpha = 0^{\circ}$ 

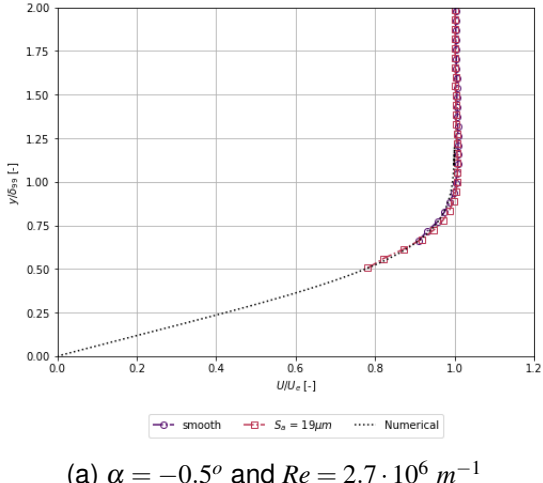
# 4. Influence of surface roughness

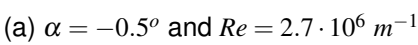
The present study examines the impact of varying surface roughness types on the boundary layer. First, a brief study on the effect of such roughness on on the mean velocity profiles is presented, followed by a discussion of their effect on the laminar-turbulent transition.

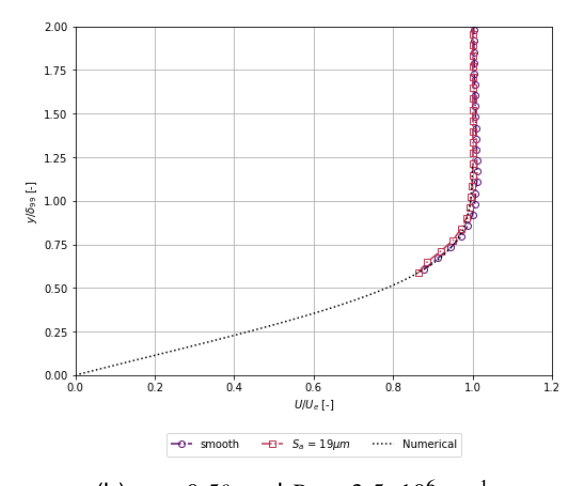
## 4.1 The mean flow

For a selected roughness,  $S_a = 19 \mu m$ , the mean velocity profiles have been measured and compared with the reference smooth case presented previously. Figure 14 illustrates this comparison for two distinct Reynolds numbers and angles of attack, demonstrating no discernible difference between the two profiles. This indicates that the limitations of the experimental setup prevent the measurement of such modifications as the starting points of the profiles are consistently positioned farther from the wall than desired. The absence of points in close proximity to the wall impedes more accurate study of the impact of surface roughness on the mean velocity profiles.

In the work of Ducaffy [11] similar difficulties encountered. Despite closer wall normal alignment of the hot-wire probe  $(y_0 \approx 50 - 100 \mu m)$  than the current study, no real change in the velocity profiles were reported. However, this is not a definite confirmation that there is no actual change in the mean velocity profiles in the presence of surface roughness. Rather, it indicates that such effect cannot be accurately measured using classical hot-wire anemometry.







(b)  $\alpha = 0.5^{\circ} \text{ and } Re = 3.5 \cdot 10^{6} \ m^{-1}$ 

Figure 14 – Boundary layer experimental-numerical comparison for the smooth reference case at x/c = 0.396

## 4.2 Instability growth and transition

As a preliminary investigation into the nature of the instabilities present, a brief spectral analysis has been conducted. However, a more comprehensive analysis will be performed in the future. Figure 15 presents the power spectral density (PSD) of u' for two different roughness heights at the same angle of attack and Reynolds numbers, with the data compared to the smooth reference case. Both cases were taken at streamwise positions in the vicinity of the onset of transition within the linear region. In both cases, an increase in the characteristic bump of the Tollmien-Schlichting is observed, which is consistent with the expected behaviour of an amplified instability due to surface roughness.

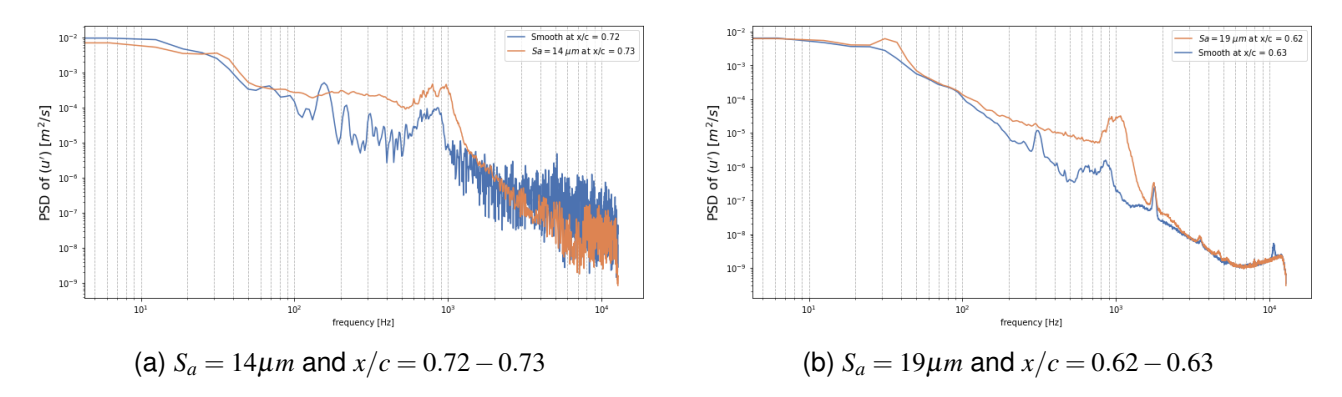


Figure 15 – PSD of u' for different roughness and  $\alpha = 0^o$  and  $Re = 3.2 \cdot 10^6 \ m^{-1}$ . Smooth reference case in blue

Figure 16 depicts the non-dimensional velocity fluctuations within the boundary layer in the streamwise direction for three roughness cases at the same Reynolds number and angle of attack. From these fluctuations, the transition positions for all the configurations are depicted, which are shown in figures 20a, 20c and 20e. As anticipated, the transition position is observed to be shifted upstream as the roughness density increases, which illustrates the significant impact that the roughness height has on transition. For relatively mild levels of roughness, the shift in transition is gradual. However, for higher roughness heights that exceed a critical value, the transition shifts rapidly to the roughness insert, rendering these cases unsuitable for the study, as this research is exclusively focused on subcritical roughness. For this reason, the majority of the results presented here focus on the roughness types with  $S_a$  values of 14 and 19  $\mu m$ . It is also important to note that in certain combinations of low-level roughness and relatively low Reynolds numbers, the effect on the transition phenomenon is minimal.

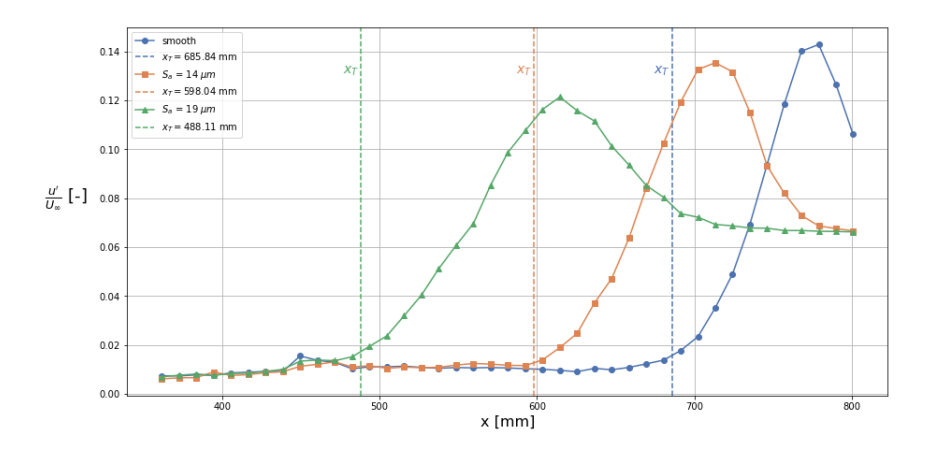


Figure 16 – Non-dimensional velocity fluctuations in the streamwise direction for different roughness types (Re =  $3.4 \cdot 10^6 \ m^{-1}$ ,  $\alpha$ =0°)

The transition positions depicted from the velocity fluctuations are then transferred to the associated N-factor envelope, which was obtained from the smooth reference case at the same Reynolds number and angle of attack. This provides the N-factor value at that specific position, which allows for the calculation of the local  $\Delta N = N_T|_{smooth} - N_T|_{rough}$  shift that the curve should encounter in order to account for the effect of the roughness on the transition without changing the  $N_T$  threshold, as specified in section 2. It is important to note that the  $\Delta N$  approach is only relevant in cases where surface roughness affects the amplification of existing instabilities, rather than in instances where the receptivity process is modified.

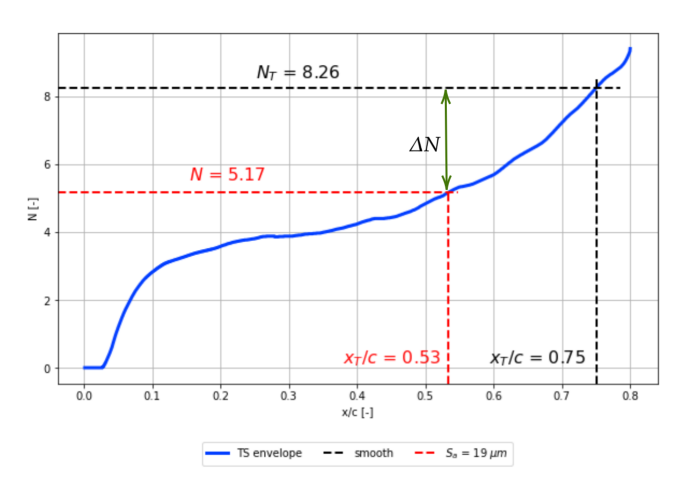
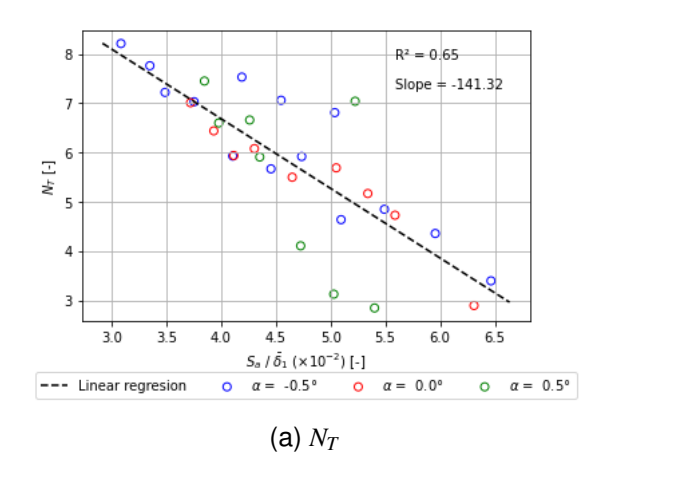


Figure 17 – N-factor and  $\Delta N$  calculated for  $S_a = 19 \mu m$  ( $\alpha = 0^o$  and Re =  $3.4 \cdot 10^6 \ m^{-1}$ )

Figures 20b, 20d and 20f illustrate the values of  $\Delta N$  obtained for  $S_a=14~\mu m$  and  $S_a=19~\mu m$ . As previously stated, the transition position for  $S_a=27\mu m$  was too advanced, particularly at high Reynolds numbers and only transition positions for Re  $<3\cdot10^6~m^{-1}$  could be calculated. As there were no reference values depicted from the smooth case, which was due to the transition occurring too downstream to be measurable, no  $\Delta N$  values could be calculated for this specific case. In these figures a rather linear dependence of  $\Delta N$  on the Reynolds number can be observed, with a higher  $\Delta N$  axis intercept for higher roughness heights. However, for  $Re>4\cdot10^6~m^{-1}$ ,  $\Delta N$  becomes rather constant with the Reynolds number. This phenomenon, previously observed by Ducaffy [11], may be linked to the close proximity of the transition position to the end of the rough area, whose distance is approximately 3.5% of the chord.



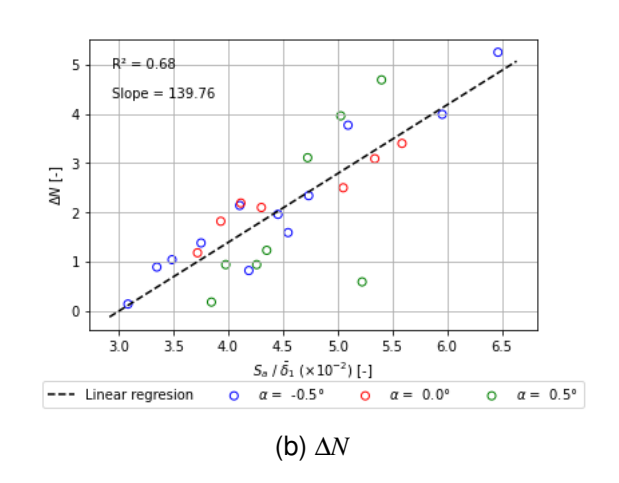


Figure 18 –  $N_T$  and  $\Delta N$  with the non-dimensional average roughness height  $S_a/\tilde{\delta}_1$  and regression lines.

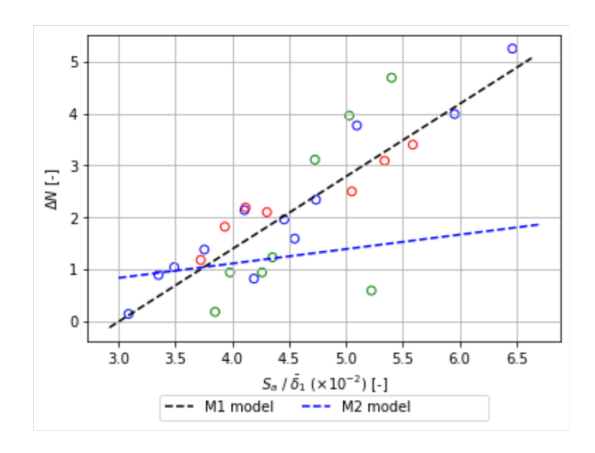


Figure 19 – Comparison of both  $\Delta N$  models

In order to facilitate the understanding of these results and enable comparison with those of previous studies [11], both the  $N_T$  values and  $\Delta N$  have been represented with respect to the dimensionless average surface roughness height  $S_a/\bar{\delta}_1$ . Here,  $\bar{\delta}_1$  corresponds to the average displacement thickness presented in figure 9. This representation allows the approximation of these results by a linear regression shown in equation 4 with  $R^2$  value of 0.68. This model shows that, for  $S_a/\bar{\delta}_1 \leq 3 \cdot 10^{-2}$  and  $\alpha = -0.5^o$  at the lowest Reynolds number (approximately  $2.5 \cdot 10^6 \ m^{-1}$ ), the value of  $\Delta N$  is zero. This result is consistent with the previous observation that certain combinations of low roughness densities and Reynolds number may not have any effect on the advancement of the transition.

$$\Delta N_{M1} = 139.76 \frac{S_a}{\overline{\delta}_1} - 4.203 \tag{4}$$

Although the proposed model offers several advantages, such as its simplicity, it is important to acknowledge its limitations. One such limitation is the dispersion of certain points considered for its modeling. It should also be noted that this model has been proposed for a very specific case and does not take into consideration the effect of the roughness streamwise extent,  $L_R$ , which has also been demonstrated to have a significant impact on the advancement of transition, as evidenced in the work of Lanzillota [21] and Ducaffy [11]. The latter proposed the  $\Delta N$  prediction model presented in equation 5, obtained from a flat plate without pressure gradient. This model depends on  $R_a/\bar{\delta}_1$  and  $L_R$  (expressed in cm), where  $R_a$  is the average roughness height over a profile, and  $\bar{\delta}_1$  has the same definition as in this paper.

$$\Delta N_{M2} = 1.86 \frac{R_a L_R}{\bar{\delta}_1} \approx 1.86 \frac{S_a L_R}{\bar{\delta}_1} \tag{5}$$

Figure 19 shows a comparison between both  $\Delta N$  models here presented. Model 1 (M1) is the model proposed in the current study, and Model 2 (M2) is the model proposed by Ducaffy in [11]. Although both exhibit some discrepancies, likely due to the dispersion of the data from which both models have been obtained, the second method tends to underestimate the  $\Delta N$  values for  $S_a/\bar{\delta}_1 > 4.5 \cdot 10^{-2}$ , and slightly overestimate it for lower roughness values. It should be noted that for the purposes of this second model, the streamwise roughness extent,  $L_R = 14.94$  cm, has been considered. Similarly, although Ducaffy's model is expressed in terms of average roughness heights measured over a profile,  $R_a$ , the surface roughness heights,  $S_a$ , were later scrutinised, as done in this paper. Finally, the consideration of an average displacement thickness may also result in some error in the non-dimensionalisation of the roughness heights, which in turn affects both models. It would be beneficial to consider alternative non-dimensionalisation techniques in the future.

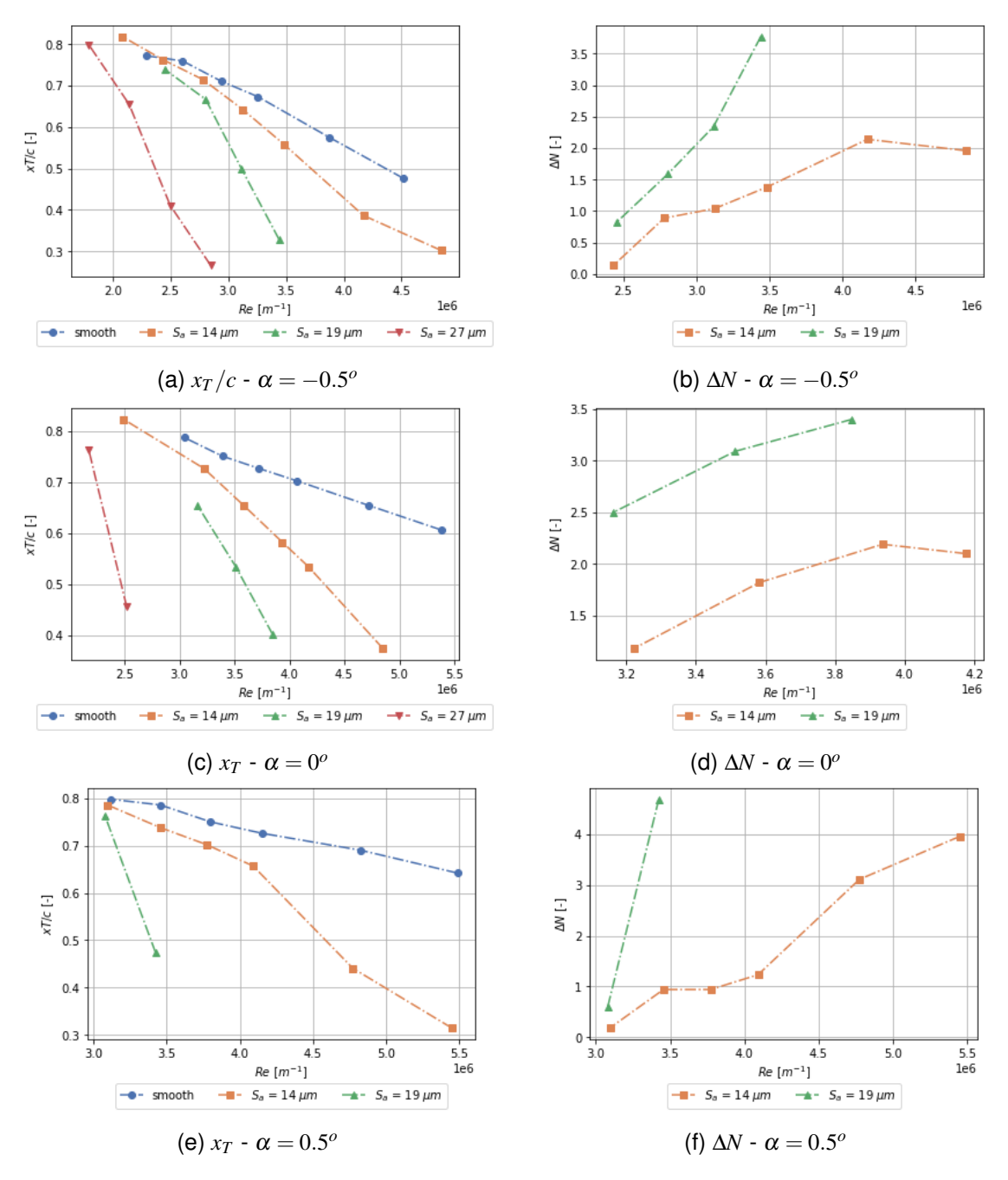


Figure 20 – Transition positions depicted for the different roughness for various Reynolds numbers

## 5. Conclusion

An experimental study was conducted to investigate the effect of surface roughness on boundary-layer transition over a swept wing. For a fixed sweep angle of  $\varphi=40^{o}$ , the results for three different angles of attack,  $\alpha=-0.5,\,0$  and  $0.5^{o}$ , have been presented at various Reynolds numbers. Firstly, measurements of the model without roughness demonstrated a satisfactory correlation with numerical values obtained using the Linear Stability Theory, with some approximation through the envelope method. These results demonstrated that the instabilities driving the transition were predominantly Tollmien-Schlichting waves. This also provided a "smooth reference case" with reference transition positions and threshold  $N_T$  values for comparison. Then, three different roughness inserts, created using sandpaper, were placed between 10% and 26.5% of the chord of the swept wing. These inserts, with average surface roughness of 14, 19 and 27  $\mu m$ , were studied for the same angles of attack and Reynolds numbers as for the reference case.

While no significant effect on the mean velocity profiles was observed, the transition positions were found to be shifted upstream in the presence of roughness, as anticipated. This allowed the investigation of the shift in the N-curve, resulting from the  $e^N$  method, that would be observed in the presence of surface roughness. The results indicated that this shift was greater for more significant roughness. This approach, which is only applicable in cases where surface roughness affects the amplification of existing instabilities, resulted in a preliminary model of the  $\Delta N = N_T|_{smooth} - N_T|_{rough}$  dependence on the dimensionless average surface roughness height,  $S_a/\bar{\delta}_1$ .

It should be noted that the semi-empirical model presented in this paper is a preliminary one that is subject to multiple limitations. Among the limitations of this model is the lack of consideration of other important roughness parameters, such as the streamwise roughness extent,  $L_R$ . It is therefore necessary to undertake further studies and to combine it with the results of different experimental campaigns' in the pipeline.

# 6. Copyright statement

The authors confirm that they, and/or their company or organization, hold copyright on all of the original material included in this paper. The authors also confirm that they have obtained permission, from the copyright holder of any third party material included in this paper, to publish it as part of their paper. The authors confirm that they give permission, or have obtained permission from the copyright holder of this paper, for the publication and distribution of this paper as part of the ICAS proceedings or as individual off-prints from the proceedings.

#### References

- [1] Gowree E, R and Atkin C, J. Excitation of instabilies in a Blasius boundary layer by surface vibration *Journal of Fluid and Structures*, Vol. 114, 103700, 2022.
- [2] Morkovin M, Reshotko E and Herbet T. Transition in open flow systems a reassessment, *Bulletin of the American Physical Society*, vol. 39, pp. 1882, 1994.
- [3] Arnal D, Perraud J and Séraudie A. Attachment line and surface imperfection problems, *Advances in Laminar–TurbulentTransition Modeling*, RTO-EN-AVT-151-09, pp. 1-20, 2008.
- [4] Methel J, Sebbane D, Forte M and Vermeersch O. Experimental study on the influence of holes on the transition on an incompressible boundary layer, *AERO2022 56th 3AF International Conference on Applied Aerodynamics*, Toulouse, France, 2022.
- [5] Beguet S, Perraud J, Forte M and Brazier J.-Ph. Modeling of transverse gaps effects on boundary-layer transition, *Journal of Aircraft*, 54:2, 794-801, 2017
- [6] Rouviere A, Pascal L, Méry F, Simon E and Gratton S. Neural Prediction Model for Transition Onset of a Boundary-Layer in Presence of 2D Surface Defects, AIAA 2022-107, AIAA SCITECH 2022 Forum, 2022.
- [7] Von Doenhoff A.E and Braslow A. L. The effect of distributed surface roughness on laminar flow, *Boundary Layer and Flow Control*, pp. 657-681, Pergamon, 1961.
- [8] Jeong H, Lee S. W and Song S.J. Measurement of transitional surface roughness effects on flat-plate Boundary layer transition, *Journal of Fluids Engineering*, vol. 141, n.7, 2019.
- [9] Crouch J, Ng L, Kachanov Y, Borodulin V and Ivanov A. Ifluence of surface roughness and free-stream turbulence oncrossflow-instability transition, *Procedia IUTAM*, vol. 14, pp. 295-302, 2015.
- [10] Ducaffy F, Forte M, Vermeersch O and Piot E. An experimental study of the effects of surface roughness on the laminar-turbulent transition of a 2D incompressible boundary-layer, AIAA 2021-0247, AIAA Scitech 2021 Forum, 2021.
- [11] Ducaffy F. Etude expérimentale de l'influence de la rugosité de surface sur la transition laminaire/turbulent d'une couche limite 2D en écoulement incompressible, PhD Thesis, *ISAE-SUPAERO*, 2022.
- [12] Reneaux J, Juillen J.C and Arnal D. Validation des critères de transition. Rapport de définition de la maquette DTP-B. Rapport final DERAT 99/5018.73, 1995.
- [13] Outtier G. Etude et fabrication de l'aile DTP-B. Rapport IMFL N° 96/76, 1995.
- [14] Teague E, Scire F.E, Baker S.M, and Jensen S.W.. Three-dimensional stylus profilometry, *Wear 83*, 1, pp. 1–12, 1982.
- [15] Smith A, Gamberoni N. Transition, Pressure Gradient and Stability Theory. *Douglas Aircraft Company*, El Segundo Division, 1956

- [16] Van Ingen J. A suggested semi-empirical method for the calculation of the boundary layer transition region. Tech. Rep. V.T.H.-74, *University of Technology, Dept. of Aero. Eng*, Delft, 1956.
- [17] Mack L.M. Boundary-layer linear stability theory, Tech. Rep. 709, AGARD, 1984.
- [18] Arnal D. Boundary layer transition: Predictions based on linear theory. Tech. Rep. Special Course on Progress in Transition Modelling, 63 p (SEE N94-33884 10-34), *AGARD*, 1994.
- [19] Arnal D. Transition prediction in transonic flow. *In Symposium Transsonicum III-IUTAM Symposium Gotlingen*, International Union of Theoretical and Applied Mechanics, Springer-Verlag, pp. 253–262, Gottingen, 1988.
- [20] Methel J. An Experimental Investigation of the Effects of Surface Defects on the Laminar Turbulent Transition of a Boundary Layer with Wall Suction, PhD thesis, *ISAE-SUPAERO*, 2019.
- [21] Lanzillotta L, Forte M and Vermeersch O. Etude expérimentale de l'influence de la rugosité de surface sur la transition laminaire/turbulent d'une couche limite incompressible. Tech. Rep. 4/23620, 2017.